Natural fault and fracture network characterization for the southern Ekofisk field
A case study integrating seismic attribute analysis with image log interpretation

Boersma, Quinten; Athmer, Wiebke; Haege, Martin; Etchebes, Marie; Haukås, Jarle; Bertotti, Giovanni

DOI
10.1016/j.jsg.2020.104197

Publication date
2020

Document Version
Final published version

Published in
Journal of Structural Geology

Citation (APA)
Boersma, Q., Athmer, W., Haege, M., Etchebes, M., Haukås, J., & Bertotti, G. (2020). Natural fault and fracture network characterization for the southern Ekofisk field: A case study integrating seismic attribute analysis with image log interpretation. *Journal of Structural Geology*, *141*, Article 104197. https://doi.org/10.1016/j.jsg.2020.104197

Journal of Structural Geology 141 (2020) 104197

Contents lists available at ScienceDirect

Journal of Structural Geology

journal homepage: http://www.elsevier.com/locate/jsg

Natural fault and fracture network characterization for the southern Ekofisk field: A case study integrating seismic attribute analysis with image log interpretation

Quinten Boersma [a,*], Wiebke Athmer [b], Martin Haege [b], Marie Etchebes [c], Jarle Haukås [b], Giovanni Bertotti [a]

[a] Delft University of Technology, Delft, the Netherlands
[b] Schlumberger Stavanger Research, Stavanger, Norway
[c] Schlumberger Doll Research, Boston, United States

ARTICLE INFO

Keywords:
Ekofisk
Fractures
Faults
Seismic attribute analysis
Image log interpretation

ABSTRACT

Production from the Ekofisk Chalk Field in the North Sea is believed to be significantly influenced by the presence of a connected fault and fracture network. In the current study, we create a 3D seismic discontinuity cube which is representative of this network within the southern part of the Ekofisk Field. This is done using a multiscale workflow which integrates seismic fault and fracture detection with borehole image log interpretation from three horizontal well sections. The results show that faults and fractures are prevalent in the Ekofisk Formations. Within the study area, faults are mainly organised in three orientations: 1) WNW-ESE, 2) NNE-SSW and 3) NNW-SSE. Smaller E-W striking faults are also observed. The interpreted fractures show a similar pattern and are organized in four orientation groups: NW-SE, WNW-ESE, ENE-WSW and NE-SW. The analysis of seismic discontinuity data (i.e. faults and fractures detectable on seismic) indicates that most small-scale discontinuities occur in proximity to large faults, and that the Lower Ekofisk Formation is characterized by more widespread – and a higher intensity of small-scale seismic discontinuities. It is also demonstrated that along each studied well section, the extracted seismic discontinuities show a qualitative correlation with the image log interpretation. This correlation suggests that the 3D seismic discontinuity cube can serve as a proxy for the fault and fracture network in the southern part of the Ekofisk Chalk Field. Following from our key findings, we conclude that the presented workflow and results could provide a starting point for future studies assessing the impact of natural fractures in the Ekofisk – and other complex reservoirs.

1. Introduction

Natural fractures play an important role in estimating the effective permeability in tight or low permeability rocks. In faulted or fractured reservoirs, these structural features may be reactivated due to continued production, resulting in unpredictable or even unwanted fluid flow behaviour such as early water breakthrough or channelized fluid flow (Jolley et al., 2007; Toublanc et al., 2005). Additionally, closed and cemented fractures can lower the effective permeability, thereby potentially inhibiting fluid flow and potential production (e.g. Bisdom et al., 2016; Laubach et al., 2019).

Predicting the geometry, location and intensity of natural fractures has become an integral component of characterizing structurally complex reservoirs. These characterization studies often consider a multitude of scales and data types (Freeman et al., 2015; Quinn et al., 2014; Williams et al., 2017). Seismic data is generally used to detect and characterize larger structural features such as faults ranging from tens to hundreds of meters (Boe, 2012; Bounaim et al., 2013; Toublanc et al., 2005). Image log - and/or core data is commonly used to detect and describe smaller structural features ranging from few centimetres to several metres. The usage of either data set in isolation has limitations with respect to its resolution. Seismic data lack the fine scale interpretation at the well location, and log data lack the lateral distribution component. However, the combination of the low-resolution seismic data and the high-resolution well data reduces the uncertainty in mapping and predicting structural discontinuities (Gauthier et al., 2002;

* Corresponding author.
E-mail address: q.d.boersma@tudelft.nl (Q. Boersma).

https://doi.org/10.1016/j.jsg.2020.104197
Received 4 September 2019; Received in revised form 10 September 2020; Accepted 11 September 2020
Available online 18 September 2020

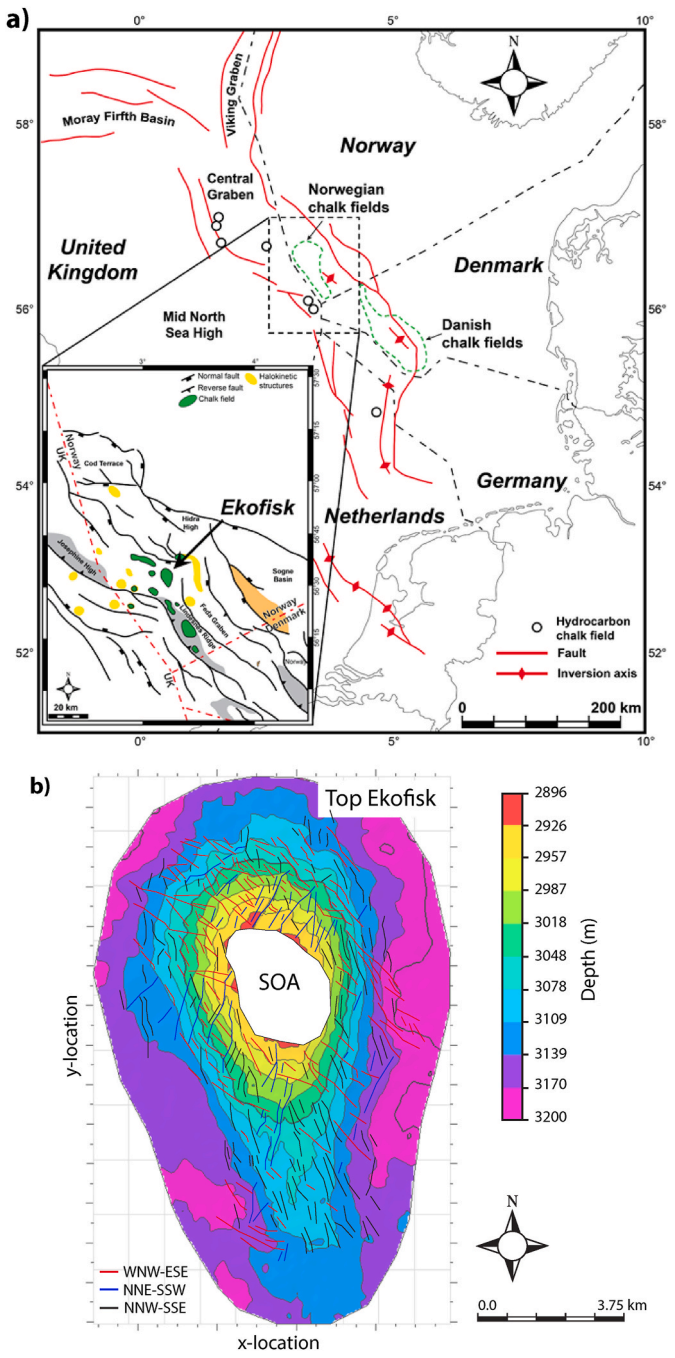

Fig. 1. Location and geometry of the Ekofisk field. a) Geographical map of the North Sea area depicting the major Mesozoic tectonic elements. Figure modified after Gennaro (2011).b) Top Ekofisk horizon and mapped fault pattern as interpreted by Toublanc et al. (2005). SOA: Seismic Obscure Area.

Laubach et al., 2019; Toublanc et al., 2005; Williams et al., 2017).

There are several published methods that allow for combining seismic and well log data with the aim to reduce prediction uncertainties. For instance, a methodology commonly used in subsurface case studies is geostatistical modelling (Gauthier et al., 2002). This method generally integrates the seismic – and borehole input data using 1) statistical distributions (e.g. fracture length or orientation), 2) large scale probability maps, and/or 3) correlations between the different datasets, in order to create large scale representations of subsurface reservoirs (e.g. Gauthier et al., 2002; Toublanc et al., 2005).

A more recent method involves the usage of linear elastic forward modelling of geologically constrained data sets, so that mechanically constrained descriptions of sub-seismic features can be realized on a reservoir scale (e.g. Boersma et al., 2019a,b; Maerten et al., 2006; Maerten et al., 2016 Maerten et al., 2019). This approach integrates seismic and well data with geological concepts such as fault or fold-related fracturing and linear elastic fracture mechanics (Maerten et al., 2006, 2019). However, successful applications of this approach require extensive knowledge of the geological and tectonic history in order to make sound assumptions.

Subsurface fracture prediction uncertainties can also be aided by outcrop analogues, which can provide valuable information on the relation between far-field stresses, local lithology, large-scale structural features (e.g. faults or folds) and local fracture-network geometries (Boersma et al., 2019a,b; Hanke et al., 2018; Maerten et al., 2016; McGinnis et al., 2015). While the importance of outcrop analogues is acknowledged, multiple studies have also shown and suggested that introducing fracture data generated under tectonic constraints different from the reservoir conditions, can introduce a considerable bias (e.g. Boro et al., 2014; Laubach et al., 2019; Sanderson, 2016; Williams et al., 2017).

Another method for characterizing naturally fractured reservoirs is to analyse attributes of high quality 3D seismic amplitude data (Bounaim et al., 2019; Jaglan and Qayyum, 2015; Williams et al., 2017). For example, edge detection attributes such as amplitude contrast or curvature can identify areas of significant changes in the seismic signal which might relate to fault zones and fracture corridors (e.g. Boe, 2012; Chopra and Marfurt, 2007; Jaglan and Qayyum, 2015). Additionally, applying edge enhancement filters allows for the automatic detection and extraction of large fault networks (Boe, 2012; Boersma et al., 2019a, b; Bounaim et al., 2013; Jaglan and Qayyum, 2015; Williams et al., 2017). Furthermore, a case study testing seismic attributes for fracture detection showed that even when being at the limit of the seismic resolution, subtle changes in the seismic signal caused by naturally fractured rock could be detected using normal-vector attributes (Bounaim et al., 2019; Haege et al., 2013). However, even though these attributes can detect fractured rock bodies, it should be noted that individual fractures interpreted from core - or image-log data fall below the resolution of the seismic attributes.

In this study, we expand the seismic reservoir characterization methodologies explained above and present a new workflow that integrates seismic fault and fracture detection with borehole image-log interpretation. This is done in order to create a 3D seismic discontinuity cube that is representative of the fault and fracture network present within the southern part of the Ekofisk Field offshore Norway, which is a large naturally fractured chalk reservoir (Fig. 1). This study is structured as follows: First, a set of newly developed seismic volume attributes and fault detection tools are presented and used to create the 3D seismic discontinuity cube. Second, small-scale structural features are interpreted and characterized using image log data from three different wells. Third, a qualitative correlation between the seismic and well data is established. Finally, the results are evaluated against 4D seismic changes caused by water injection and the implications and potential for future work are discussed.

2. Geological setting and study area

2.1. Tectonic setting and stratigraphy

The Ekofisk field is located in the southern part of the Norwegian Central Graben (NCG) which represents the southern branch of the North Sea triple rift system (Gennaro, 2011) (Fig. 1a). The present configuration of the NCG is the result of several subsequent tectonic events (Gennaro, 2011; Vejbæk and Andersen, 2002; Ziegler, 1990, 1992):

1) WNW-ESE Permo-Triassic extension and the deposition of the Zechstein successions

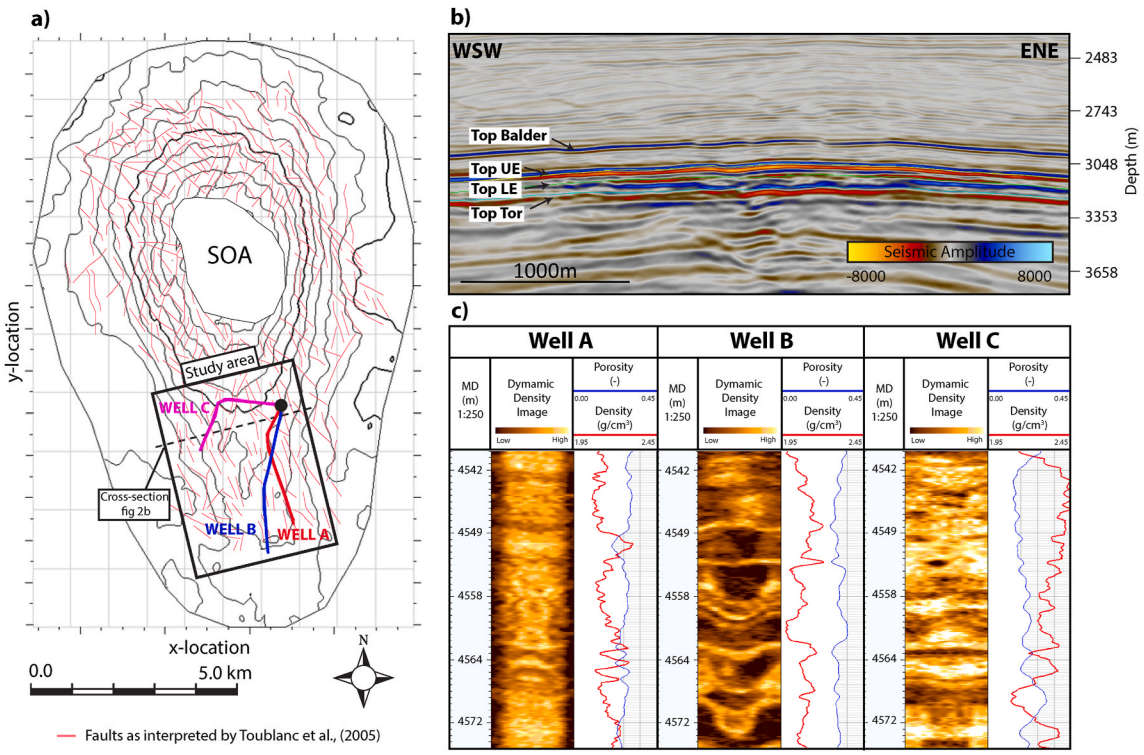

Fig. 2. Dataset and study area. a) Location of the study area. Contour lines represent the top Ekofisk horizon and range from 2900 m at the crest to 3200 m at the fringes. The 3D seismic data have been cropped by the extend of the study area. The colour coding of the three wells will be applied throughout this study. Faults mapped on top Ekofisk. (modified after Toublanc et al., 2005). b) Cross section through study area. Note that the key formations have been marked (Balder, Upper Ekofisk FM (UE), Lower Ekofisk (LE) and Tor. c) Subset of the azimuthal density image logs used for the fracture and fault interpretation.

2) Early Jurassic doming
3) Late Jurassic rifting (WNW-ESE extension)
4) Early Cretaceous E-W compression (inversion) and transpressive movement along NW-SE Triassic-Jurassic faults
5) Late Cretaceous to Eocene thermal subsidence accompanied by several NNE-SSW compressive pulses resulting in the inversion of major basement faults and salt movement
6) Continued halokinesis and the development 4-way dip anticlines (domes)

The Ekofisk Chalk Field is a dome structure (Fig. 1a and b) comprising upper Cretaceous and lower Paleogene reworked chalk sediment of the Tor Formation, the Lower Ekofisk Formation and the Upper Ekofisk Formation (Gennaro et al., 2013). These formations are overlain and sealed by the silt and shale layers of the Paleogene Balder Formation, resulting in large entrapments of hydrocarbons.

2.2. Field characteristics

The Ekofisk reservoir rocks exhibit relatively high porosities (±30%) and comparatively low matrix permeabilities ranging between 0.1 and 10 mD (Gennaro et al., 2013; Tolstukhin et al., 2012; Toublanc et al., 2005). Also, as known from other chalk fields in the North Sea (e.g. Klinkby et al., 2005), a gas cap at the crest of the field produces a Seismically Obscured Area (SOA) within the centre of the dome and in younger stratigraphic layers (Fig. 1b). A vast network of connected faults and fractures exists in the chalk formations, which significantly enhances the effective permeability of the normally tight reservoir rocks (up to 50mD), thereby making commercial production possible (Agarwal et al., 1997; Teufel and Farrell, 1990; Toublanc et al., 2005).

Previous seismic interpretations point out that the Ekofisk fault network shows three main orientations (WNW-ESE, NNW-SSE, NNE-SSW) (Gennaro, 2011; Jones et al., 2014; Toublanc et al., 2005) (Fig. 1b). Fracture classification studies using core data indicate that the Ekofisk fracture network can be sub-divided into four main classes, namely: 1) Tectonic fractures, 2) stylolite-associated fractures, 3) irregular fractures and 4) healed fractures, with the tectonic fractures being most dominant and the main contributors to the effective permeability within the Ekofisk reservoir formations (Agarwal et al., 1997; Jones et al., 2014; Teufel and Farrell, 1990; Toublanc et al., 2005). The main orientations of these small-scale structural features are commonly sub-divided in three main sets which generally strike parallel to the orientations of the main fault groups (i.e. WNW-ESE, NNW-SSE, NNE-SSW) (Agarwal et al., 1997; Teufel and Farrell, 1990; Toublanc et al., 2005). This observation has led to the assumption that the Ekofisk faults and fractures are structurally related (Agarwal et al., 1997; Teufel and Farrell, 1990; Toublanc et al., 2005).

3. Methodology

3.1. The dataset

This study focuses on the southern part of the Ekofisk Chalk Field, outside of the SOA (Fig. 2a). This part of the field was chosen, such that potential sources of knowable seismic noise (e.g. production patterns, acquisition geometry (i.e. edge of the survey) and SOA) were best avoided.

The studied dataset consists of post-stack 3D seismic amplitude data and azimuthal density borehole image logs from three horizontal wells (Fig. 2a, b and c). The 3D seismic amplitude data were acquired prior to the onset of injection in the southern part field in 2014. The seismic data has binsize dimensions of 12.5 m by 12.5 m by 3.06 m. At reservoir depth, the vertical resolution and horizontal resolution were estimated to be 19 m and 63 m (determined with the point spread function), respectively. Reservoir markers such as the Top Balder and Top Upper Ekofisk can be identified (Fig. 2b). In addition to the 3D seismic data, a

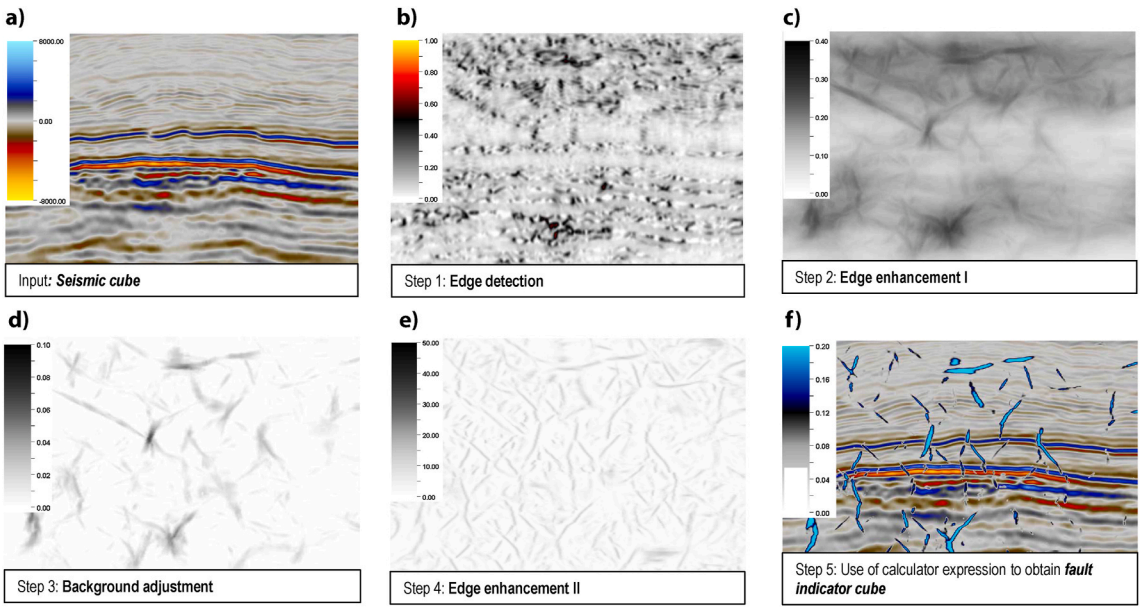

Fig. 3. Large scale discontinuity (e.g. faults) detection and extraction workflow: a) Seismic input cube. b) Edge detection using the amplitude contrast filter (step 1). c) Edge enhancement with a 3D energy orientation filter (EEI) (step 2). d) Background adjustment using the Gaussian horizontal mean (step 3). e) Further enhancement to detect ridges (EEII) (step 4). f) Scaling and normalizing the edges (step 5). Note that the exact calculator expression is confidential. See the text for additional details on the workflow and different attributes.

4D time-strain cube (i.e. the time-shift of the seismic signal caused by changes in the reservoir properties (e.g. Rickett et al., 2007)) was used to evaluate how faults and fractures impact production (section 5.2). This 4D time-strain cube was created by combining two seismic cubes, which were acquired at different times (i.e. prior to injection and production and during active injection and production).

The three horizontal wells investigated in this study (wells A, B and C) were drilled into the Upper - and Lower Ekofisk Formation, respectively (Fig. 2a) (Well A: Upper Ekofisk and Well B & C: Lower Ekofisk). These wells are currently being utilized as injectors. The three respective azimuthal density image logs (ALD) have a relatively low resolution (i.e. vertical sampling ALD = 15.24 cm with respect to the vertical sampling of high-resolution FMI = 0.254 cm). This makes the interpretation of small scale and individual fractures difficult (Fig. 2c). However, while the resolution is low these logs can be used to identify larger features (fractured or faulted rocks) showing distinct changes in the rock density (Fig. 2c) (e.g. Ibrayev et al., 2016).

3.2. Large-scale seismic discontinuity analysis

Faults detectable on seismic data were detected using five edge attributes (Aqrawi and Boe, 2011; Boe, 2012; Bounaim et al., 2013) (Fig. 3): 1) edge detection with a dip-guided 3D Sobel attribute, 2) edge enhancement with a 3D Radon filter, 3) background adjustment, 4) additional edge enhancement (ridge detection attribute) and 5) scaling of edges using a voxel-by-voxel arithmetic calculation. The edges attributes were conditioned in such a way that only structural elements with a measurable seismic displacement were detected.

The first step in this workflow was edge detection using a dip-guided 3D Sobel attribute (Amplitude Contrast) (Fig. 3b) (Aqrawi and Boe, 2011). This attribute highlights areas where the seismic amplitude is disturbed or displaced and could therefore indicate faults, changes in depositional environment, or the reworking of sediments. In the second step, the seismic signature of medium-to large-scale faults was enhanced by subsequently applying a 3D Radon filter (Edge Enhancement 1) (Boe, 2012) (Fig. 3c). This filter enhanced planar seismic features by iteratively comparing, summing, averaging and smoothing the discontinuities (i.e. results of step 1) along planes with arbitrary dips and dip-directions (bounds of the allowed plane rotations are defined by the user), so that larger 3D discontinuities were enhanced, while smaller features, such as noise, were smoothed away (Boe, 2012). The third step involved the adjustment of the background, i.e. subtracting the Gaussian horizontal mean from the enhanced edge cube (Fig. 3d). In the fourth step, another edge enhancement step was performed to detect ridges (Edge Evidence attribute in Petrel) (Fig. 3e). Finally, the seismic cubes from steps 3 and 4 were multiplied, using a dataset specific best practice approach (i.e. calculator expressions formations were dependent on the input data and output discontinuity cubes) (Step 5) (Fig. 3f). The resulting discontinuity cube was then normalized, such that larger and wider faults have values close to 1.0, while subtle discontinuities are represented by values ranging between 0.2 and 0.6. Areas without faults or discontinuities have values close to zero. The normalized discontinuity cube was used to characterize the large faults within the Ekofisk Field.

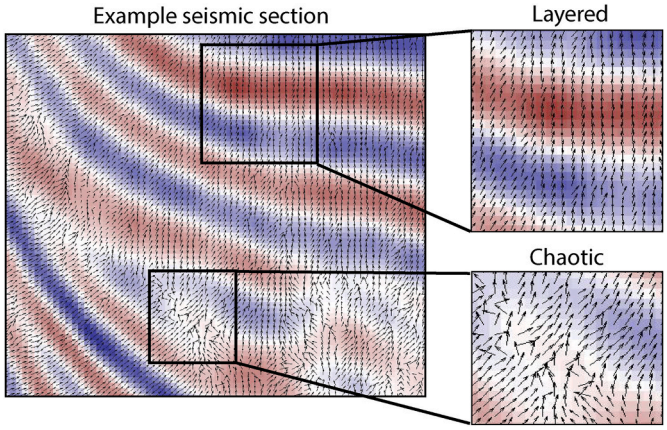

Fig. 4. Normal vector field overlaid on a seismic section. Layered and chaotic seismic signals are clearly identified by differences in the behaviour of the normal vector field. Figure modified from Bounaim et al. (2019). Note that the depicted seismic data are an example and do not represent seismic data used in study.

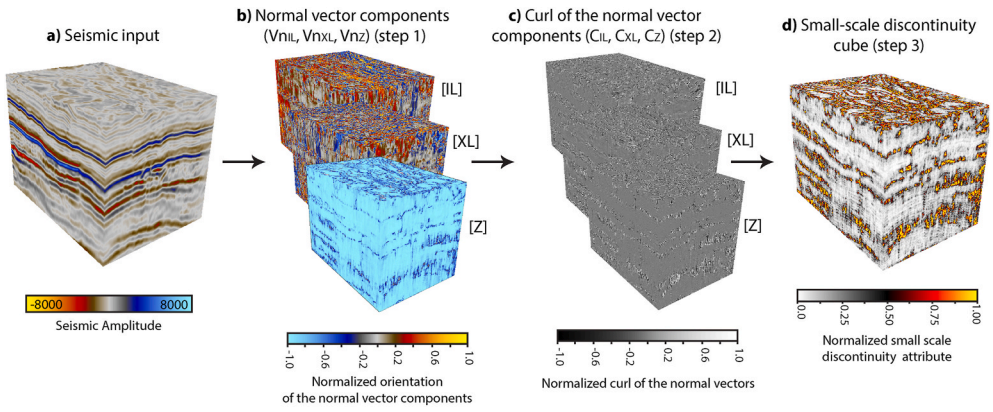

Fig. 5. Sequence of steps used for the small-scale discontinuity detection and characterization. The cubes shown in this figure have the same size as the 3D seismic data utilized and presented within this stud. Comparison of the discontinuity cubes project on top of the Ekofisk horizon is shown later in the results section (e.g. Figs. 7–9). a) Input seismic reflection data. b) Normal vectors of the seismic data in three dimensions (Vn_{IL} (inline), Vn_{XL} (crossline) and Vn_Z (vertical)). c) Curl attribute of the three normal vector components (C_{IL}, C_{IL} and C_Z). d) Magnitude of the curl attribute components (i.e. $M = \sqrt{C_{IL}^2 + C_{XL}^2 + C_Z^2}$) which was normalized. See the text for additional details on the workflow and different attributes.

3.3. Small-scale seismic discontinuity analysis

Small-scale discontinuities (e.g. fractured rock) were more difficult to detect using the contrast in seismic amplitude. For this reason, these discontinuities were detected using 3D seismic vector attributes (Bounaim et al., 2019; Haege et al., 2013) (Fig. 4). This approach consists of the calculations of three subsequent volume attributes: 1) Normal vector calculations, 2) computation of the curl attribute and 3) computation of the small-scale seismic discontinuity cube (Fig. 5) (Bounaim et al., 2019; Haege et al., 2013).

The first step in the small-scale discontinuity analysis was the computation of the normal vectors of the seismic data in the three seismic components (Figs. 4 and 5a-b (step 1)). Here, the normal vector field was generated using a polynomial reconstruction of the seismic signal (Sonneland et al., 1998), which allowed for calculation of derivatives in each direction (inline, crossline, vertical). For consistency, the vectors were normalized to unit length and point upwards (Fig. 4). These three components of the normal vector field (Vn_{IL}, Vn_{XL} and Vn_Z) were used to calculate the dip and azimuth of the small scale discontinuities (Bounaim et al., 2019). In the second step, the curl of the normal-vector components was computed (Fig. 5c). This attribute captured abrupt spatial changes (rotation) in the normal vector data within each seismic voxel, thereby making it very effective in detecting subtle changes in the seismic reflection data (Bounaim et al., 2019). The final step involved the computation of the magnitude of the three curl attribute components (Step 3) (Fig. 5d). This magnitude cube was proven to be efficient for identifying fractured rock in a previous case study (Haege et al., 2014) and will be used for characterizing small scale discontinuities (e.g. fractured rock) throughout this study.

3.4. Fracture interpretation from borehole image logs

The three aforementioned azimuthal density image logs were analysed using the Schlumberger Techlog wellbore software platform. Fractures were interpreted using a consistent resolution (1:100 (MD)), as features showing abrupt changes in the density and porosity log as well as clear changes in the borehole image log itself (i.e. both an increase and a decrease with respect to the background data) (Fig. 2c). Because of the quality and type of the utilized borehole data (Fig. 2c), discrimination between the different structural features present within the Ekofisk reservoir formations (i.e. tectonic fractures, stylolite-associated fractures, irregular fractures, and healed fractures) was impossible. Therefore, the interpreted features will collectively be called fractures throughout this paper. However, we acknowledge that this is a simplification that should be addressed in future studies, since the structural discontinuities present within the Ekofisk reservoir formations have different mechanical origins and have a distinct impact on the effective permeability (Peacock et al., 2016; Toublanc et al., 2005).

From the interpreted fracture data, the Terzaghi corrected fracture intensity (P10) along the different wells was calculated (Fig. 6a) (Terzaghi, 1965). Subsequently, the computed P10 was smoothed using a constant sampling window of 122 m (400 ft) (Fig. 6b). Such a large sampling window was chosen so that zones of intensively fractured rock could be identified and compared to the seismic discontinuity data.

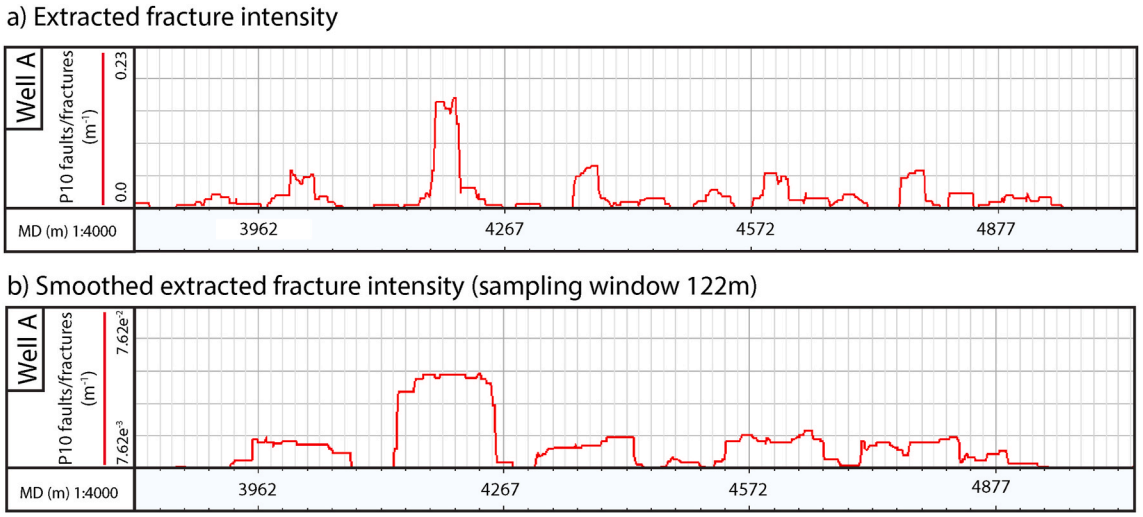

Fig. 6. Smoothing the fracture intensity data. a) Interpreted fracture intensity (P10) for well A. b) Smoothed fracture intensity using a sampling window of 122.0 m.

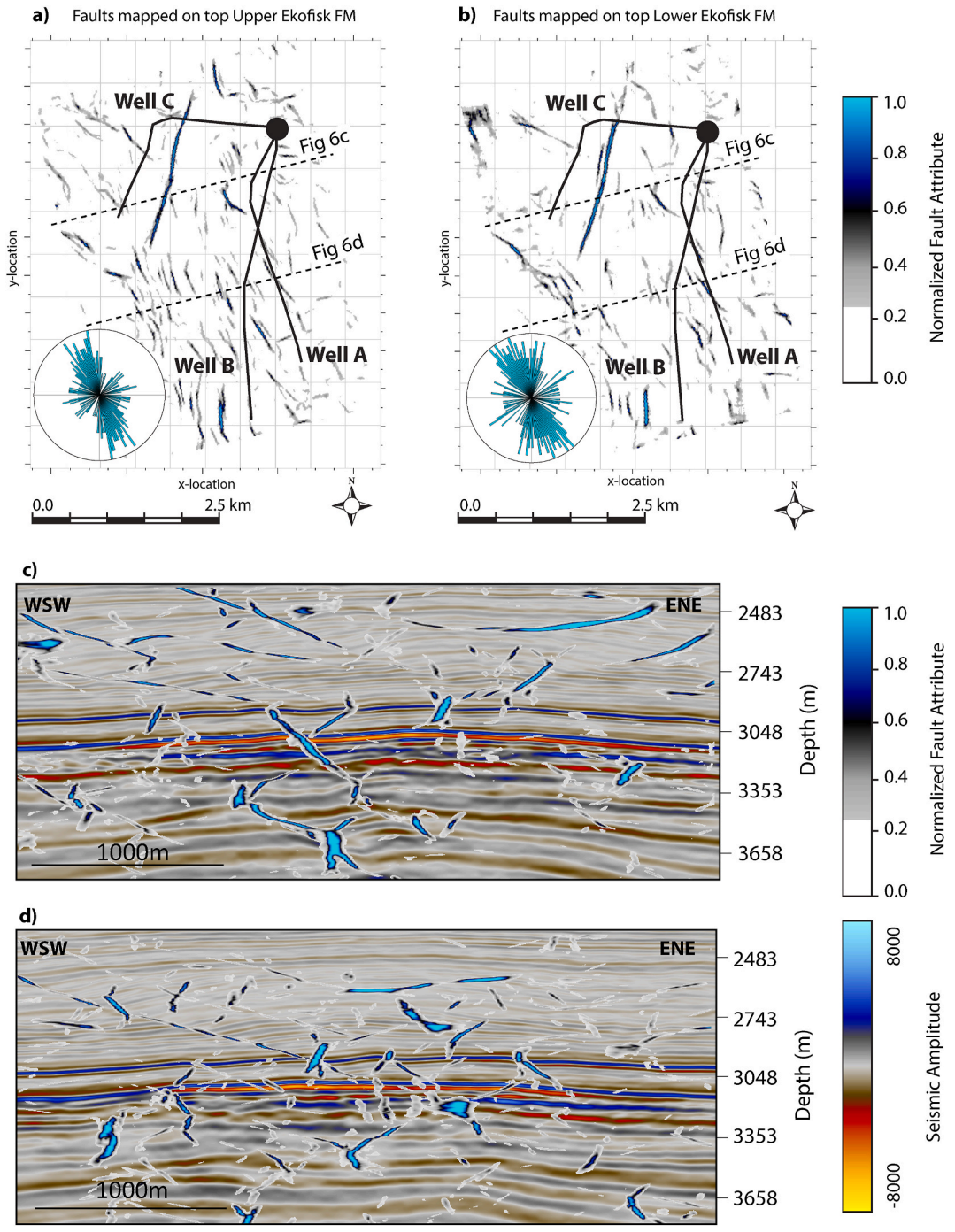

Fig. 7. Results of the seismic fault characterization workflow. a-b) Faults extracted from the seismic depicted on the Upper and Lower Ekofisk formations, respectively. Number of interpreted faults used for the rose diagram are 152 for the upper Ekofisk and 122 for the lower Ekofisk. c-d) Two WSW-ESE cross sections through the seismic data with extracted faults. Note that for this figure, faults having an attribute value lower than 0.225 are not shown (see section 3.2.). Further, because of the 2D planar depiction, faults which strike parallel to the cross section, have an apparent dip which is parallel to the bedding.

Apart from the fracture intensity, the orientation distributions of the interpreted fractures were acquired for each well.

3.5. Well to seismic correlation

To assess the correlation between the seismic attributes and the interpreted well data, the results of the seismic discontinuity analysis, i.e. small- and large-scale seismic-discontinuity cubes, were extracted along each well. This was done using the well-seismic tool in Petrel and data was extracted along a 40 m wide plane which was parallel to the trajectory of each analysed well (see Petrel manual for additional information on the data extraction). Subsequently, the extracted seismic data were compared to the interpreted fracture intensity and orientation, so that a qualitative correlation could be established.

4. Results

4.1. Large-scale discontinuity detection

The results of the seismic fault detection workflow (Fig. 3) indicate

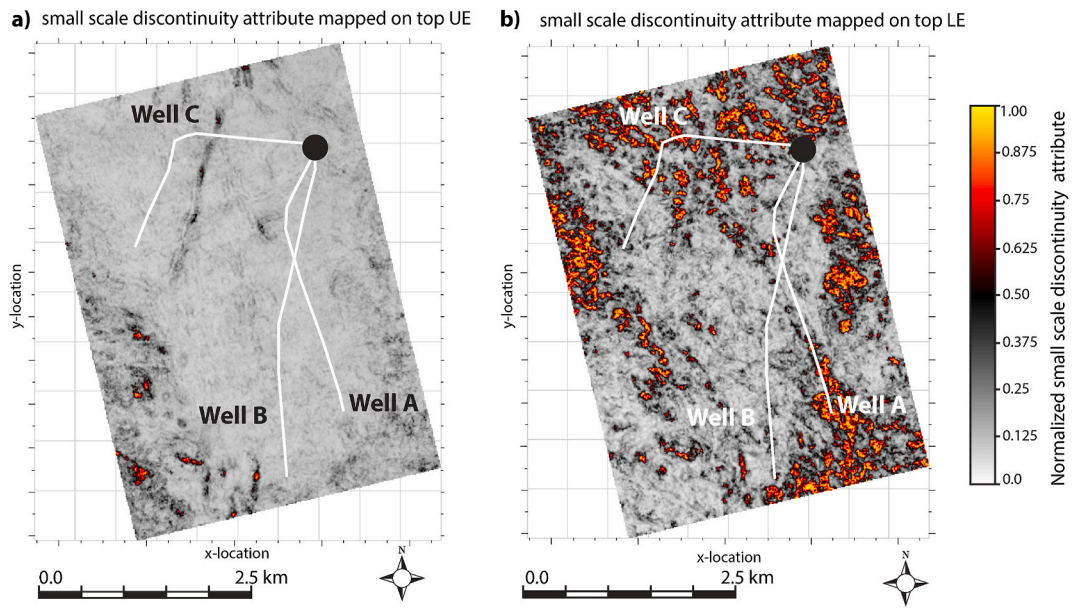

Fig. 8. Results of the small-scale discontinuity workflow. a-b) Small-scale discontinuity attribute (SCDA) mapped on top of the Upper and Lower Ekofisk formations, respectively.

that the Upper - and Lower Ekofisk Formation are heavily faulted (Fig. 7a–b), with the extracted faults showing three main orientations: 1) NNW-SSE, 2) NNE-SSW, and 3) WNW-ESE. Smaller E-W faults are also observed (Fig. 7a–b). For simplicity these E-W faults have been categorized in the WNW-ESE group.

The WNW-ESE fault group is believed to be linked to the underlying WNW-ESE striking Jurassic rift faults and mainly occurs in clustered zones in the northern and western part of the study area (Fig. 7a–b). Faults within the WNW-ESE fault group show relatively low displacement values and are generally not observed within the overlying Balder Formation (Fig. 7a–d). The locality of the clustered WNW-ESE fault zones is consistent with previous interpretations of the Ekofisk fault network (e.g. Toublanc et al., 2005) (Fig. 2a).

The dominant NNW-SSE faults strike parallel to the major hinge axis of the Ekofisk dome structure. These faults are thought to be related to major doming events, and are most dominant in the Upper Ekofisk - and Balder Formation (Fig. 7a–d). Within the Lower Ekofisk Formation, the dominance of the NNW-SSE fault group is less apparent (Fig. 7a–d). Faults belonging to the NNW-SSE fault group show both inversion and normal faulting, implying that this fault group has been affected by the Late Cretaceous to Eocene NNE-SSW compressive events (Fig. 7c–d) (Gennaro, 2011).

The NNE-SSW fault group is easily detectable from the seismic data. It shows normal displacement and is present throughout the Ekofisk - and Balder Formation (Fig. 7). These NNE-SSW faults displace the Ekofisk dome structure, suggesting that they continued to be active after the major doming events. Similarly to was observed in previous fault interpretations (e.g. Toublanc et al., 2005) our results show that this fault group is mainly clustered near the centre of the dome (Figs. 1b and 7).

4.2. Small-scale discontinuity analysis

The analysis of small-scale discontinuities indicates that for the Upper Ekofisk Formation, the highest discontinuity attribute magnitudes (values ranging between 0.25 and 0.70) can be found in proximity to the larger NNE-SSW faults and along the WNW-ESE fault corridor (Figs. 7a and 8a). The areas in proximity to NNW-SSE and other smaller faults show magnitudes slightly higher than 0.15 (i.e. dark grey features). Apart from the faulted areas, the attribute map shows relatively low values (i.e. magnitudes lower than 0.15) (Fig. 8a), which most likely implies that apart from faulted areas, very few small-scale discontinuities are present within the Upper Ekofisk Formation.

The Lower Ekofisk Formation shows more detectable small-scale seismic discontinuities (Fig. 8b). Again, the results indicate that high-attribute values occur along large fault planes present within the Lower Ekofisk Formation (e.g. the NNE-SSW - and WNW-ESE faults) (Fig. 8a–b). However, the results also show that within the Lower Ekofisk Formation, areas which show high discontinuity magnitudes exist in locations where no faults are detected (Figs. 7b and 8b). For example, in the northern and western edges of the study area, large WNW-ESE and NW-SE elongated discontinuities are present in areas where only a few large faults were extracted (Figs. 7b and 8b). The orientation of these small-scale features is roughly parallel to the faults that are in proximity, and this could imply that they represent small structural features such as fracture corridors (Figs. 7b and 8b). However, in the southern and eastern edges of the study area, these features do not seem to align with the local fault orientations (Figs. 7b and 8b). A possible explanation for this observation is that within these areas, the small-scale discontinuities represent debris flows which are known to be present within the Lower Ekofisk – and Tor Formation (Gennaro et al., 2013). Alternatively, these discontinuities could represent an artifact in the utilized Lower-Ekofisk horizon.

4.3. The combined seismic discontinuity cube

For the Ekofisk Field, the faults and tectonic fractures are believed to be structurally related (i.e. fault-related fracturing) (Agarwal et al., 1997; Toublanc et al., 2005). This implies that within our workflow both the large- and small-scale discontinuity cubes (Figs. 7 and 8) can be associated with fractured or faulted zones.

Therefore, to create a representative discontinuity cube, the results of the small- and large-scale discontinuity analysis are normalized and added together. The resulting cube is called the seismic discontinuity cube and this cube is representative for both large- and small-scale discontinuities (e.g. faults and fractures) which are detectable from seismic (Fig. 9a–d). This cube will be used for further evaluation against the image log data.

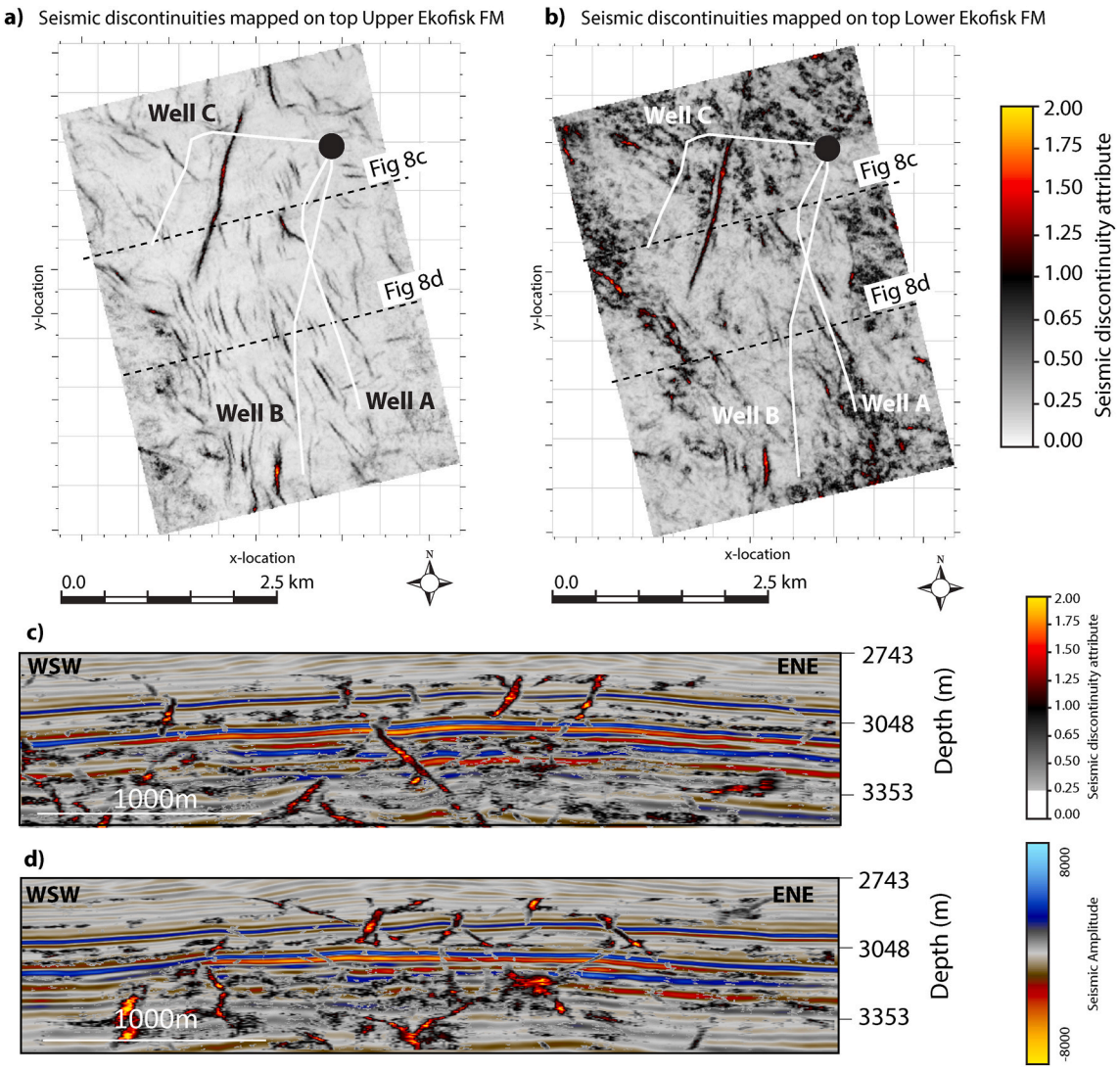

Fig. 9. Seismic discontinuity attribute (SDA) (i.e. summation of small- and large-scale discontinuity cubes). a-b) Seismic discontinuity attribute mapped on top the Upper and Lower Ekofisk FM's, respectively. c-d) Two WNW-ESE cross sections through the seismic data and extracted discontinuity cubes.

4.4. Borehole image log interpretation

The borehole image log interpretation results show similar orientations with respect to the faults detected on the seismic (i.e. NNW-SSE -, NNE-SSW -, WNW-ESE - and smaller E-W faults) (Figs. 7 and 10a-b). Based on the measured orientation, the interpreted fractures can be subdivided into four groups, namely: NW-SE, WNW-ESE, ENE-WSW, and NE-SW (Fig. 10a–b). The dip data indicate that 81% of the interpreted fractures have a dip ranging between $45° \leq$ dip $\leq 90°$ (Fig. 10a–b), verifying that the interpreted features mainly represent tectonic fractures (e.g. Agarwal et al., 1997; Jones et al., 2014; Teufel and Farrell, 1990; Toublanc et al., 2005).

Discriminating the fracture data per well shows that each well is characterized by two fracture orientations (Table 1, Fig. 10a–b). The orientation distributions of wells A and B highlight that the most dominant fracture groups strike approximately NW-SE and NE-SW (Table 1, Fig. 10a–b). The similarities between the two wells are expected because wells A and B are both located in the southern part of the study area and drilled sub-parallel to each other (Fig. 2a). Moreover, seismic discontinuities in proximity to these two wells show similar orientations to those interpreted in the image logs (Fig. 7a–b, 9a-b and 10 a-b). Well C is characterized by NNW-SSE and E-W striking fractures (Fig. 10a–b and Table 1). Again, these fracture orientations are also observed in the seismic discontinuity data in proximity to well C (Fig. 7a–b, 9a-b and 10 a-b).

Although extracted fracture groups show similar orientation with respect to the seismic discontinuity data, it should be noted that fractures striking parallel to the well orientation are most likely undersampled and under-represented in the acquired orientation distribution (Fig. 10b). This implies that for wells A and B, the NNW-SSE striking features and for well C, the NE-SW striking fractures are underrepresented because they strike parallel to the respective well trajectory (Fig. 10b).

The borehole image log interpretation also indicates that most fractures show clustering behaviour and that fractures can be grouped in different zones showing relatively high intensity magnitudes (Fig. 6a–b and 10c-d) (Sanderson and Peacock, 2019). For Well A, the interpretation indicates that five different zones of relatively high intensity fracturing could be identified (Fig. 10c–d). The intensity distribution for well B shows that the different fractures clusters can be grouped in two distinct zones, that are separated by a relatively long interval which shows almost no fracturing (Fig. 10c–d). Well C, has a more continuous fracture intensity signal and the results indicate that the interpreted features can roughly be sub-divided into two separate zones (Fig. 10c–d).

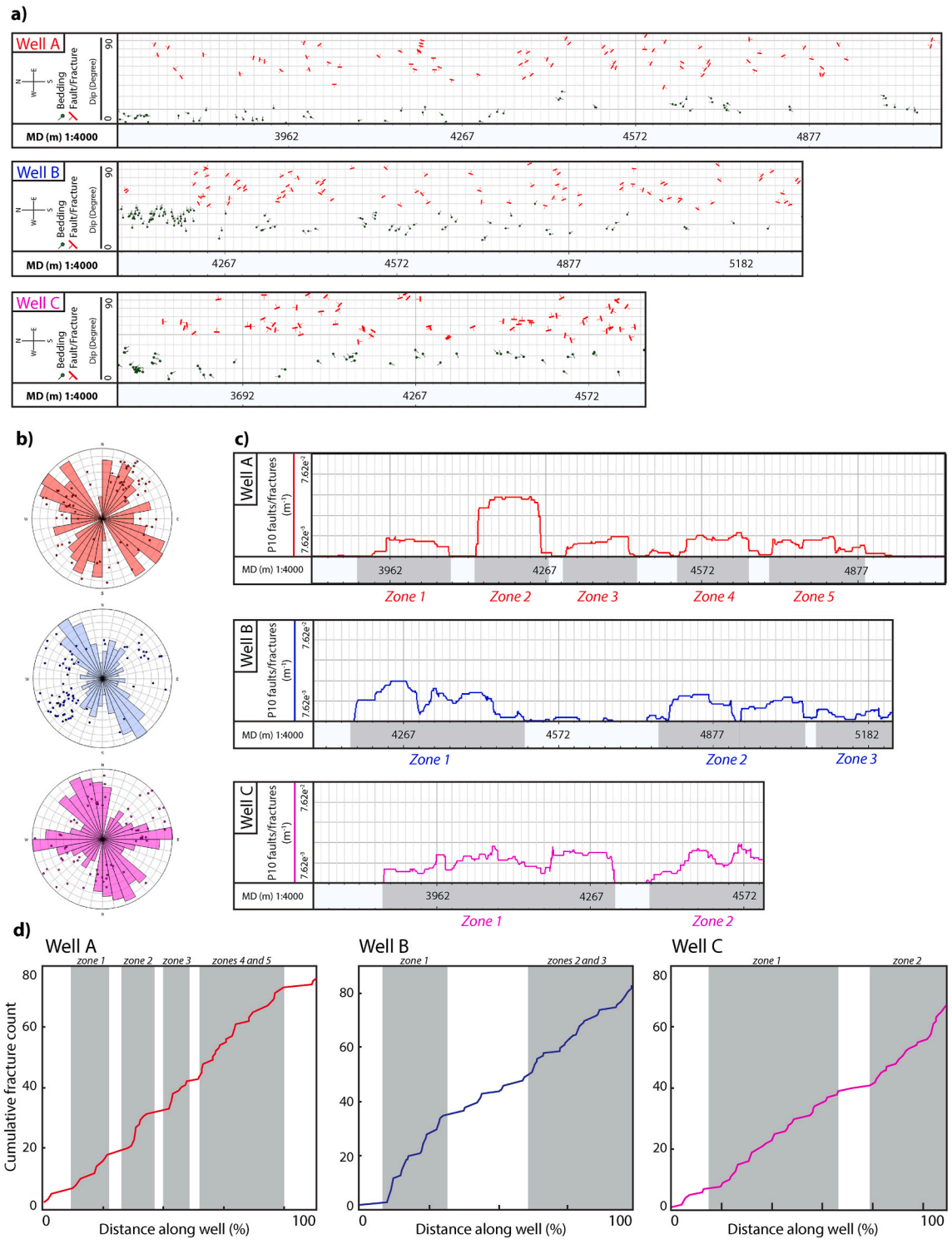

Fig. 10. Image log interpretation results. a) Tad poles of the interpreted beddings and fractures along each well. b) Extracted orientation distribution and pole data, c) smoothed fracture intensity distributions (P10), and d) Cumulative plots of fracture count vs. distance (%) for wells A, B and C, respectively. Note that the different wells are also indicated by their respective colour. Furthermore, see Figs. 2, 7 and 8 or 9 for the location of the wells. (For interpretation of the references to colour in this figure legend, the reader is referred to the Web version of this article.)

4.5. Comparison between image logs and seismic discontinuity data

The extraction of seismic data along each well, allows for the comparison of the seismic discontinuity cube and interpreted image log data (Fig. 11a–b). The results indicate that for well A, the peaks in the interpreted fracture intensity distribution have a good qualitative fit with the peaks in the seismic discontinuity signal, with most of the high intensity zones being captured by the seismic discontinuity cube. Well B has a reasonable fit between the seismic discontinuity data and interpreted fracture intensity distribution. Here, the different zones of fracturing are captured by the seismic discontinuity cube. The seismic signal extracted along well C shows a signal with two distinct peaks, which roughly correlate with the centres of the two interpreted fracture zones. This implies that well C also shows a reasonable qualitative correlation

Table 1
Interpreted fracture groups and extracted orientation data from the seismic along each well used in this study.

Well	Interpreted fracture groups	Extracted strike data from seismic
Well A	NW-SE, NE-SW, E-W (weakest signal)	E-W, NW-SE, NNW-SSE, NE-SW
Well B	NW-SE, NE-SW	NNW-SSE, NE-SW
Well C	NNW-SSE, E-W, NE-SW (minor signal)	NW-SW, ENE-WSW, NE-SW

with the seismic data (Fig. 11a–b).

While a qualitative correlation is observed, discrepancies between the interpreted fracture intensity and seismic signal are also noted (Fig. 11a–b). For example, in well B, the start and measured intensity of the first fracture zone has not fully been captured by the seismic discontinuity cube. Furthermore, the peak in the seismic discontinuity signal observed at MD = 4420 m does not fully coincide with a peak in fracture intensity (Fig. 11b). In well C, the two distinct fracture zones are not fully captured by the seismic discontinuity data (Fig. 11a–b). These observed differences could potentially be explained by the seismic resolution or uncertainties in the velocity model. For instance, some of the interpreted fractures could fall below the seismic resolution. Furthermore, due to uncertainties in the velocity model, small discrepancy between the depth of the well data and depth of the seismic could exist.

By extracting the azimuth data of the seismic discontinuity cubes (i.e. can be computed from the three normal vector components (Fig. 5b)) along each well, the orientation distributions of the interpreted fractures and the seismic discontinuities can be compared. The results show that for all wells, the dominant orientations observed in the image logs are also observed and sampled in by the seismic discontinuity cube (Fig. 12a–c and Table 1) (i.e. Well A: NW-SE, NE-SW, E-W, well B: NW-SE, NE-SW and well C: NW-SE, E-W). Furthermore, the orientation distribution from the seismic data highlights an additional fracture group (Fig. 11a–c). This group strikes parallel to the well trajectory and could therefore not be sampled by the image log interpretation (Fig. 12a–c and Table 1) (i.e. NNW-SSE for well A and B and NE-SW for well C).

However, as was observed with the fracture intensity correlation, small discrepancies between the orientation distributions do exist. Here, a possible explanation for the differences could be the resolution of the available image logs, which is relatively low (Fig. 2), potentially impacting the accuracy of the actual interpretation and thereby of the measured fracture orientations. Another possible explanation is that the seismic and well data sample the observed structural features in different proportions.

In summary, our results show that the seismic and well data show a qualitative correlation, emphasizing that the seismic discontinuity cube can be used for identifying zones of relatively high-density fracturing (Figs. 10 and 11). Additionally, the orientation data in the discontinuity cube can be utilized to identify the dominant strike of the fractured zones (Figs. 5 and 12).

5. Discussion

5.1. A seismic-driven workflow for characterizing natural faults and fractures in the Ekofisk Field

In complex reservoirs such as the Ekofisk Field understanding the spatial distribution, geometry and intensity of natural fracture and fault systems is seen as an integral component in predicting the effective permeability and potential fluid flow patterns (Agarwal et al., 1997; Haukås et al., 2018; Jones et al., 2014; Teufel and Farrell, 1990; Tolstukhin et al., 2012, 2014; Toublanc et al., 2005). Here, fractures and faults are believed to greatly enhance the permeability of the normally tight chalk rocks, making production possible (e.g. Agarwal et al., 1997; Toublanc et al., 2005). Therefore, to better predict fluid-flow behavior during production, several attempts have been made to map the fracture intensity and effective permeability using a variety of methods. For instance, Toublanc et al. (2005) used mappable faults and empirical relations to create reservoir scale fracture intensity and effective permeability models. Agarwal et al. (1997) used a positive relationship between matrix porosity and fracture intensity to map the effective permeability. A more recent method involves the inclusion of 4D seismic data in order to update existing reservoir models (e.g. Tolstukhin et al., 2014; Tolstukhin et al., 2012).

This study used a seismic-driven workflow to characterize the spatial distribution of the natural fault and fracture network present within the southern Ekofisk Field. The workflow comprises of newly developed seismic attributes (Boe, 2012; Bounaim et al., 2013, 2019; Haege et al., 2013; Haukås et al., 2018) in order to detect large-scale (e.g. faults) and small-scale discontinuities (e.g. fractures rock). The resulting discontinuity cubes show fault orientations and network geometries which are comparative to previous fault interpretations (e.g. Toublanc et al., 2005), acknowledging that the presented workflow could be utilized for extracting structural features up to the resolution of the seismic data. Further, the discontinuities detected on the seismic highlighted qualitative correlations with fracture data interpreted from the available image logs (Figs. 11 and 12), which implies that the presented seismic discontinuity cube could be used for identifying zones of relatively high intensity fracturing and faulting.

However, while the qualitative correlation between the seismic and well data holds valuable information, a direct – and quantitative correlation between the two datasets was not observed (Fig. 11). This implies that improvements to the workflow and results are necessary before the seismic discontinuity cubes can be used as quantitative input for modelling the tectonic fracture network at reservoir level. These improvements can range from adding steps to the seismic discontinuity workflow (see section 5.3) to introducing core - and higher resolution borehole image data (e.g. Teufel and Farrell, 1990; Toublanc et al., 2005), thereby: 1) reducing the uncertainties in the extracted seismic discontinuities, and 2) better characterizing the different structural features present within the Ekofisk reservoir formations (i.e. tectonic fractures, stylolite-associated fractures, irregular fractures, and healed fractures).

Another possible improvement is to do a more in-depth analysis of the available image log - and seismic discontinuity data. For example, the interpreted fracture intensity (P10) and the observed seismic discontinuity data could be differentiated by orientation (Figs. 10–12), so that a better geological understanding between the small- and large-scale structural features is achieved. By doing so, the presented results could potentially be fitted to different fault damage zone models, thereby allowing for the translation of seismic discontinuity data to different fault/fracture probability models (e.g. Gauthier et al., 2002; Mayolle et al., 2019; Toublanc et al., 2005).

5.2. Potential implications for the Ekofisk field and other complex reservoir studies

We propose that the presented workflow and results can improve the characterization of the Ekofisk and other complex reservoir studies. For instance, the extracted seismic discontinuity cube can help in identifying zones which have a high probability of being significantly faulted or fractured. Furthermore the presented discontinuity cubes could be evaluated against dynamic data such as 4D seismic, which measures the change in seismic behaviour (i.e. time shift, amplitude and impedance) caused by production or injection over time (e.g. Folstad, 2016; Tolstukhin et al., 2014; Tolstukhin et al., 2012). (Folstad, 2016; Haukås et al., 2018)

For the Ekofisk reservoir formations, negative seismic changes (i.e. 4D seismic hardening) are generally associated with 1) an increase of the water saturation, 2) rock compaction, 3) pressure depletion, and 4) channelized fluid flow caused by the presence of natural faults and

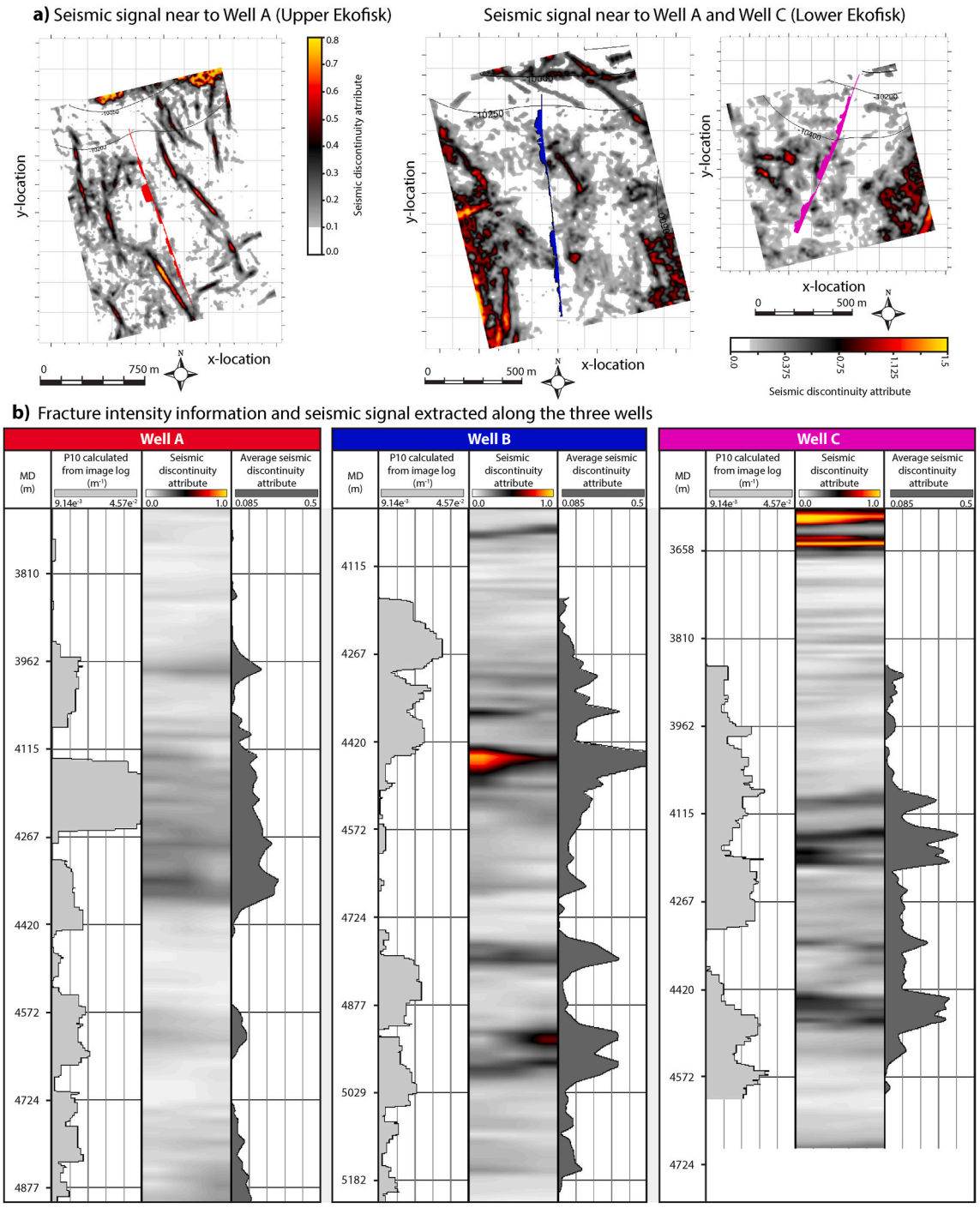

Fig. 11. Comparison between the observations made using the seismic data and data extracted from the three wells. a) Seismic discontinuity signal and well information depicted on a surface which is parallel to the respective well (i.e. surface is extracted from the well path). Note that the relative fracture intensity has been plotted on top of each well trajectory and that well B and C share the same colour bar. b) Measured fracture intensity and seismic discontinuity signal extracted along each well respectively. Width of extraction was 40 m (20 m either side) for each well (see section 3.5). (For interpretation of the references to colour in this figure legend, the reader is referred to the Web version of this article.)

fractures. This implies that, along actively injecting wells, the 4D seismic hardening data should show similar patterns as the seismic discontinuities and natural fractures. Therefore, to better understand whether such a correlation exists, seismic hardening data were extracted along a plane parallel to Well B (active injector well) and projected on top of the seismic discontinuity cube (Fig. 13). The depicted 4D changes represent the difference in two seismic datasets after 4 years of water injection. This figure shows that in most areas close to the trajectory of Well B, the 4D anomalies follow the general trend observed in the seismic discontinuity cube. This geometric fit suggests that the seismic discontinuity cube is representative of faults and fractures which increase the effective permeability and therefore channel fluid flow.

While a geometric overlap between the two datasets exists, further research is needed to fully understand the correlation between observable discontinuities and 4D seismic changes. Therefore, we propose that the seismic discontinuity cube can provide a starting-point for an ensemble-based 4D seismic history-matching workflow as suggested by Haukås et al. (2018) or Tolstukhin et al. (2014). Here, the seismic

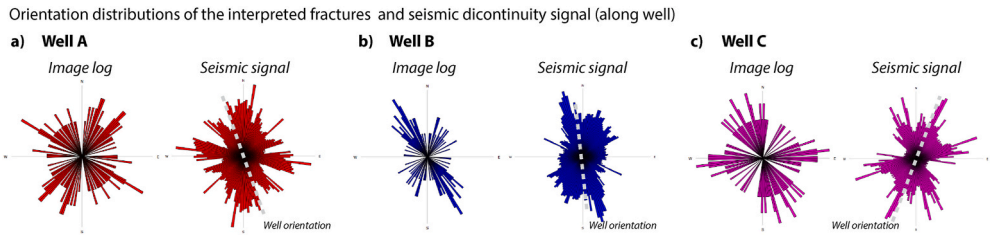

Fig. 12. a-c) Orientation distributions acquired from the image log interpretation and extracted seismic data for wells A, B and C, respectively. Azimuth results are extracted directly along the well (no averaging).

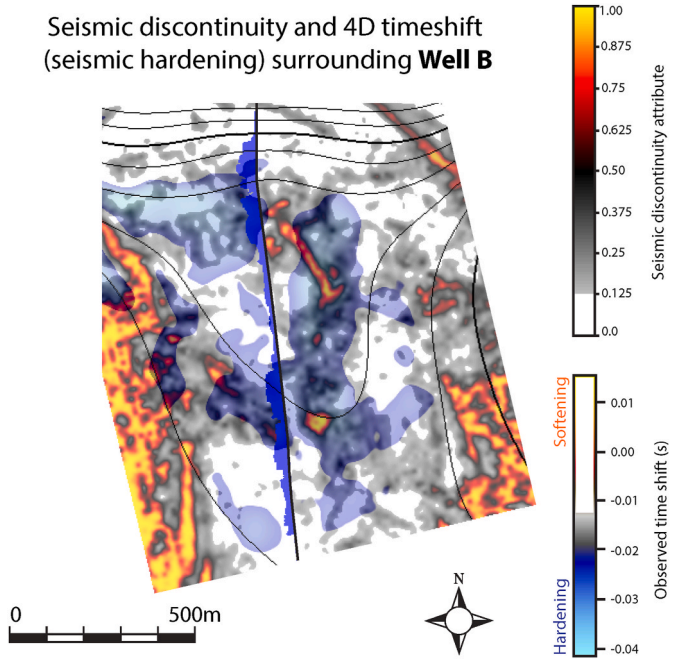

Fig. 13. Seismic discontinuity cube and 4D seismic changes (seismic hardening after 4 years of injection) depicted on a surface which is parallel to Well B. Note that the log parallel to Well B represents the local fracture intensity (Fig. 10c). Further it should be noted that seismic softening has been filtered.

discontinuity cube can be used to generate different effective permeability and/or discrete fracture network models which can be implemented into dynamic reservoir simulations. The results of these simulations can then be compared to production data at the wells or to 4D changes observed in the seismic, so that geologically constrained reservoir models can be generated.

5.3. Potential improvements to the small-scale seismic discontinuity workflow

Attributes using the rotation of normal vectors calculated from the seismic data could be used for the detection of small-scale discontinuities which fall at the limit of the seismic resolution (Bounaim et al., 2019; Haege et al., 2013). In this study, these attributes were used for detecting intensively fractured rock. However, because these attributes use subtle rotations in the seismic data for discontinuity detection, they could be very sensitive to random seismic noise, which may lead to erroneous results and/or interpretations. Therefore, to minimize this potential issue in future studies, we suggest that signal to noise studies should be conducted, so that the sensitivity of the small-scale discontinuity workflow in relation to seismic noise is better assessed and quantified.

Another improvement to the workflow concerns sedimentary features such as debris or mass flows. These deposits are known to be present within the Ekofisk - and Tor Formation (Gennaro et al., 2013) and due to their dipping beds, may well cause distinct rotations in the seismic data. This implies that using the current settings of the small-scale discontinuity analysis, these sedimentary structures could well be present within the seismic discontinuity cubes. The extraction of sedimentary features could potentially explain the high discontinuity magnitudes that were detected in areas where no large-scale faults were observed (e.g. southern and eastern edges of the Lower Ekofisk Formation) (Figs. 7 and 8). Therefore, to avoid the potential extraction of discontinuities caused by sedimentary structures in future studies, we propose that an additional vertical dip filter can be implemented to the small-scale discontinuity workflow.

6. Conclusions

This study implements a workflow of seismic-discontinuity extraction and image log-interpretation, in order to create a 3D seismic discontinuity cube which is representative of the fault - and fracture network present within the southern part of the Ekofisk Chalk Field, offshore Norway.

The results of the seismic discontinuity analysis show that extracted faults mainly show three orientations, namely: NNW-SSE, NNE-SSW, and WNW-ESE. Apart from these three main orientations, smaller E-W striking faults are also observed. These observed fault orientations are consistent with earlier interpretations presented in literature.

The results of the small-scale discontinuity analysis indicate that most detectable features occur in proximity to – or follow the orientation of larger-scale faults present within the study area. The results also show that within the Upper Ekofisk Formation, very few small-scale discontinuities are present away from larger faults. Within Lower Ekofisk Formation the small-scale discontinuities are more widespread and show higher magnitudes.

The image log interpretation indicates that fractures depict a similar pattern with respect to the extracted faults, and show four main orientations, namely: NW-SE, WNW-ESE, ENE-WSW and NE-SW. The extracted dip data ranges between 45° and 90°, thereby suggesting that most of the interpreted fractures belong to the tectonic fracture group. The conducted intensity analysis shows that fractures mainly occur in clusters. These clusters mostly concentrate in larger separated zones showing relatively high fracture intensity.

At the well locations the extracted seismic discontinuity-cube shows a qualitative correlation with the interpreted fracture data, with most of the interpreted fracture zones being captured by the seismic discontinuity cube. Further, for all studied wells, the computed orientation of the seismic discontinuities is similar to the orientation of the interpreted fractures. Moreover, at the location of well B, the interpreted fractures and extracted seismic discontinuities show a geometric fit with 4D seismic hardening effects caused by four years of injection.

Finally, based on presented results, we suggest that the seismic discontinuity cube is most likely representative for faults and fractures which actively channel fluids within the Ekofisk Field. Therefore, we propose that the presented workflow and results could be utilized in

future projects in order to better assess the impact of natural faults and fractures within the Ekofisk Chalk Field and other structurally complex reservoirs. However, it should be noted that improvements to the workflow and presented dataset are necessary before such a feat can be fully achieved.

CRediT authorship contribution statement

Quinten Boersma: Software, Formal analysis, Project administration, Conceptualization, Writing - review & editing, Visualization, Data interpretation. **Wiebke Athmer:** Software, Formal analysis, Project administration, Conceptualization, Writing - review & editing, Supervision, Data interpretation, Data gathering. **Martin Haege:** Software, Formal analysis, Writing - review & editing, Data interpretation. **Marie Etchebes:** Software, Project administration, Conceptualization, Formal analysis. **Jarle Haukås:** Software, Project administration, Conceptualization, Formal analysis, Writing - review & editing, Data gathering. **Giovanni Bertotti:** Project administration, Conceptualization, Writing - review & editing, Supervision.

Declaration of competing interest

The authors declare that they have no known competing financial interests or personal relationships that could have appeared to influence the work reported in this paper.

Acknowledgements

We would like to thank ConocoPhillips for providing the data. The authors acknowledge the Research Council of Norway and the industry partners, ConocoPhillips Skandinavia AS, Aker BP ASA, Vår Energi AS, Equinor ASA, Neptune Energy Norge AS, Lundin Norway AS, Halliburton AS, Schlumberger Norge AS, and Wintershall DEA, of The National IOR Centre of Norway for support. Further, we thank the Schlumberger Stavanger Research Team for providing key technologies used in this project. We also express our gratitude to Tanja Kontsedal for introducing the borehole image log interpretation software used in this study. Finally, we would like to acknowledge the team of ConocoPhillips Skandinavia for reviewing this work. We note however that the opinions presented are those of the authors and do not necessarily represent those of ConocoPhillips Skandinavia AS. This research is indeed partly funden by the IOR centre. My PhD has been funded by Dutch Top-Sector for Upstream gas (project no. TKI01020IG).

References

Agarwal, B., Allen, L.R., Farrell, H.E., 1997. Ekofisk field reservoir characterization: mapping permeability through facies and fracture intensity. SPE Form. Eval. 12, 227–234. https://doi.org/10.2118/35527-PA, 04.

Aqrawi, A.A., Boe, T.H., 2011. Improved fault segmentation using a dip guided and modified 3D Sobel filter. In: SEG Technical Program Expanded Abstracts 2011, pp. 999–1003. https://doi.org/10.1190/1.3628241.

Bisdom, K., Bertotti, G., Nick, H.M., 2016. The impact of different aperture distribution models and critical stress criteria on equivalent permeability in fractured rocks. J. Geophys. Res.: Solid Earth 121, 4045–4063. https://doi.org/10.1002/2015JB012657.Received.

Boe, T.H., 2012. Enhancement of large faults with a windowed 3D Radon transform filter. SEG Tech. Progr. Expand. Abstr. 1–5. https://doi.org/10.1190/segam2012-1008.1, 2012.

Boersma, Q., Athmer, W., Etchebes, M., Haukås, J., Bertotti, G., 2019a. Natural Fracture Prediction: A Multiscale Integration of Seismic Data, Image Logs and Numerical Forward Modelling. In: 81st EAGE Conference & Exhibition, pp. 3–6.

Boersma, Q., Prabhakaran, R., Bezerra, F.H., Bertotti, G., 2019b. Linking natural fractures to karst cave development: a case study combining drone imagery, a natural cave network and numerical aperture modelling. Petrol. Geosci. https://doi.org/10.1144/petgeo2018-151.

Boro, H., Rosero, E., Bertotti, G., 2014. Fracture-network analysis of the Latemar Platform (northern Italy): integrating outcrop studies to constrain the hydraulic properties of fractures in reservoir models. Petrol. Geosci. 20 (1), 79–92. https://doi.org/10.1144/petgeo2013-007.

Bounaim, A., Bø, T.H., Athmer, W., Sonneland, L., Knoth, O., 2013. large fault extraction using point cloud approach to a seismic enhanced discontinuity cube. 75th EAGE Conference & Exhibition 2013, London, pp. 10–13.

Bounaim, Aicha, Etchebes, M., Haukås, J., Borgos, H., Fotland, B.H., Sonneland, L., 2019. Vector attributes - a family of advanced seismic attributes to assist in geological interpretation. In: SEG International Exposition and Annual Meeting 2019, pp. 1813–1817. https://doi.org/10.1190/segam2019-3214107.1.

Chopra, S., Marfurt, K.J., 2007. Volumetric Curvature Attributes Adding Value to 3D Seismic Data Interpretation, vol. 2007. Society of Exploration Geophysicists - 77th SEG International Exposition and Annual Meeting, SEG, pp. 851–855, 2002.

Folstad, P.G., 2016. Monitoring of the Ekofisk Field with 4D Seismic Data from a Permanently Installed Seafloor System. In: IOR Norway: Recover for the Future.

Freeman, B., Quinn, D.J., Dillon, C.G., Arnhild, M., Jaarsma, B., 2015. Predicting subseismic fracture density and orientation in the gorm field, Danish North Sea. Geol. Soc. Lond. Spec. Publ. 421 (1), 231–244. https://doi.org/10.1144/SP421.9.

Gauthier, B.D.M., Garcia, M., Daniel, J.M., 2002. Integrated fractured reservoir characterization: a case study in a North Africa field. SPE Reservoir Eval. Eng. 5 (4), 284–294. https://doi.org/10.2118/79105-PA.

Gennaro, M., Wonham, J.P., Saelen, G., Walgenwitz, F., Caline, B., Fay-Gomord, O., 2013. Characterization of dense zones within the danian chalks of the Ekofisk field, Norwegian North Sea. Petrol. Geosci. 19 (1), 39–64. https://doi.org/10.1144/petgeo2012-013.

Gennaro, Matteo, 2011. 3D seismic stratigraphy and reservoir characterization of the chalk group in the Norwegian central graben, North Sea. University of Bergen. https://bora.uib.no/handle/1956/5393.

Haege, M., Maxwell, S., Sonneland, L., Norton, M., 2013. Rock fabric characterization using 3D reflection seismic integrated with microseismic. In: 75th European Association of Geoscientists and Engineers Conference and Exhibition 2013 Incorporating SPE EUROPEC 2013: Changing Frontiers, pp. 4897–4901. https://doi.org/10.3997/2214-4609.20130214.

Haege, Martin, Maxwell, S., S, L., Norton, M., 2014. New 3-D seismic vector attribute explains hydraulic fracture behavior (March). Retrieved from. http://www.slb.com/~/media/Files/pts/industry_articles/201403_aogr_characterize_rock_fabric_shale.pdf.

Hanke, J.R., Fischer, M.P., Pollyea, R.M., 2018. Directional semivariogram analysis to identify and rank controls on the spatial variability of fracture networks. J. Struct. Geol. 108 (January 2017), 34–51. https://doi.org/10.1016/j.jsg.2017.11.012.

Haukås, J., Athmer, W., Bakke, J.O.H., Boersma, Q.D., Bounaim, A., Etchebes, M., et al., 2018. Analysis of Enhanced Permeability Using 4D Seismic Data and Locally Refined Simulation Models. In: IOR: Reservoir & Production Management Conference. Norwegian Petroleum Society.

Ibrayev, F., Fernandez-Ibanez, F., DeGraff, J.M., 2016. Using a genetic-based approach to enhance natural fracture characterization in a giant carbonate field. In: Society of Petroleum Engineers - SPE Annual Caspian Technical Conference and Exhibition. https://doi.org/10.2118/182565-ru, 2016.

Jaglan, H., Qayyum, F., 2015. Unconventional seismic attributes for fracture characterization. First Break 33 (March), 101–109.

Jolley, S.J., Barr, D., Walsh, J.J., Knipe, R.J., 2007. Structurally complex reservoirs: an introduction. Geol. Soc. Lond. Spec. Publ. 292 (1), 1–24. https://doi.org/10.1144/SP292.1.

Jones, G.A., Kendall, J.M., Bastow, I., Raymer, D.G., Wuestefeld, A., 2014. Characterization of fractures and faults: a multi-component passive microseismic study from the Ekofisk reservoir. Geophys. Prospect. 62 (4), 779–796. https://doi.org/10.1111/1365-2478.12139.

Klinkby, L., Kristensen, L., Nielsen, E.B., Zinck-Jørgensen, K., Stemmerik, L., 2005. Mapping and characterization of thin chalk reservoirs using data integration: the Kraka Field, Danish North Sea. Petrol. Geosci. 11 (2), 113–124. https://doi.org/10.1144/1354-079304-632.

Laubach, S.E., Lander, R.H., Criscenti, L.J., Anovitz, L.M., Urai, J.L., Pollyea, R.M., et al., 2019. The role of chemistry in fracture pattern development and opportunities to advance interpretations of geological materials. Rev. Geophys. 1–47. https://doi.org/10.1029/2019rg000671.

Maerten, L., Gillespie, P., Daniel, J.M., 2006. Three-dimensional geomechanical modeling for constraint of subseismic fault simulation. AAPG (Am. Assoc. Pet. Geol.) Bull. 90 (9), 1337–1358. https://doi.org/10.1306/03130605148.

Maerten, L., Legrand, X., Castagnac, C., Lefranc, M., Joonnekindt, J.-P., Maerten, F., 2019. Fault-related fracture modeling in the complex tectonic environment of the Malay Basin, offshore Malaysia: an integrated 4D geomechanical approach. Mar. Petrol. Geol. 105, 222–237. https://doi.org/10.1016/j.marpetgeo.2019.04.025.

Maerten, L., Maerten, F., Lejri, M., Gillespie, P., 2016. Geomechanical paleostress inversion using fracture data. J. Struct. Geol. 89, 197–213. https://doi.org/10.1016/j.jsg.2016.06.007.

Mayolle, S., Soliva, R., Caniven, Y., Wibberley, C., Ballas, G., Milesi, G., Dominguez, S., 2019. Scaling of fault damage zones in carbonate rocks. J. Struct. Geol. 124 (2018), 35–50. https://doi.org/10.1016/j.jsg.2019.03.007.

McGinnis, R.N., Ferrill, D.A., Smart, K.J., Morris, A.P., Higuera-Diaz, C., Prawica, D., 2015. Pitfalls of using entrenched fracture relationships: fractures in bedded carbonates of the hidden valley fault zone, Canyon Lake Gorge, Comal County, Texas. AAPG (Am. Assoc. Pet. Geol.) Bull. 99 (12), 2221–2245. https://doi.org/10.1306/07061513012.

Peacock, D.C.P., Nixon, C.W., Rotevatn, A., Sanderson, D.J., Zuluaga, L.F., 2016. Glossary of fault and other fracture networks. J. Struct. Geol. 92, 12–29. https://doi.org/10.1016/j.jsg.2016.09.008.

Quinn, D., Freeman, B., Dillon, C., Arnhild, M., Jaarsma, B., 2014. Building a robust framework model for geomechanical prediction of fracture density, orientation and likely hydraulic signature: leading-edge technology in the Gorm field Danish Central

Graben. SEG Tech. Progr. Expand. Abstr. 1528–1532. https://doi.org/10.1190/segam2014-0148.1, 2014.
Rickett, J.E., Duranti, L., Hudson, T., Regel, B., Hodgson, N., 2007. 4D time strain and the seismic signature of geomechanical compaction at genesis. In: 69th European association of Geoscientists and Engineers Conference and Exhibition 2007: Securing the Future. Incorporating SPE EUROPEC 2007, 6, pp. 3448–3452. https://doi.org/10.3997/2214-4609.201401441.
Sanderson, D.J., 2016. Field-based structural studies as analogues to sub-surface reservoirs. Geol. Soc. Lond. Spec. Publ. 436 (1), 207–217. https://doi.org/10.1144/SP436.5.
Sanderson, D.J., Peacock, D.C.P., 2019. Line sampling of fracture swarms and corridors. J. Struct. Geol. 122 (December), 27–37. https://doi.org/10.1016/j.jsg.2019.02.006, 2018.
Sonneland, L., Tennebo, P. O., Gehrmann, T., Oyvind, Y., Steen Boge, K., & Berge, G. (1998). WO1998037437A1.
Terzaghi, R.D., 1965. Sources of error in joint surveys. Geotechnique 15 (3), 287–304. https://doi.org/10.1680/geot.1965.15.3.287.
Teufel, L.W., Farrell, H.E., 1990. Situ Stress and Natural Fracture Distribution in the Ekofisk Field, North Sea. In: AAPG Annual Conference, pp. 1–33, 1990.
Tolstukhin, E., Hu, L.Y., Sudan, H.H., 2014. Geologically consistent seismic history matching workflow for Ekofisk chalk reservoir. In: 14th European Conference on the Mathematics of Oil Recovery 2014, ECMOR, vol. 2014, pp. 8–11. https://doi.org/10.3997/2214-4609.20141781. September 2014.
Tolstukhin, Evgeny, Lyngnes, B., Sudan, H.H., 2012. Ekofisk 4D seismic - seismic history matching workflow. In: SPE Europec/EAGE Annual Conference, pp. 4–7. https://doi.org/10.2118/154347-MS.
Toublanc, A., Renaud, S., Sylte, J.E., Clausen, C.K., Eiben, T., Nådland, G., 2005. Ekofisk Field: fracture permeability evaluation and implementation in the flow model. Petrol. Geosci. 11 (4), 321–330. https://doi.org/10.1144/1354-079304-622.
Vejbæk, O.V., Andersen, C., 2002. Post mid-cretaceous inversion tectonics in the Danish Central Graben - regionally synchronous tectonic events? Bull. Geol. Soc. Den. 49 (2), 139–144.
Williams, R.M., Pascual-Cebrian, E., Gutmanis, J.C., Paton, G.S., 2017. Closing the seismic resolution gap of fractures through seismic and image-log analysis, a North Sea case study. Interpretation 5 (3), SJ21–SJ30. https://doi.org/10.1190/INT-2016-0163.1.
Ziegler, P.a., 1992. North Sea rift system. Tectonophysics 208 (1–3), 55–75. https://doi.org/10.1016/0040-1951(92)90336-5.
Ziegler, P.A., 1990. Geological atlas of Western and Central Europe. The Hague: Shell Internationale Petroleum Maatschappij. Distributed by Geological Society Pub. House.